

Part II

Measurement and Calibration of Fringe Parameters

Chapter 7

Visibility Estimation and Calibration

M. MARK COLAVITA

JET PROPULSION LABORATORY
CALIFORNIA INSTITUTE OF TECHNOLOGY
PASADENA, CALIFORNIA

7.1 Introduction

Fringe visibility is the fundamental observable in interferometric imaging, as it is related to the object brightness via the van Cittert–Zernike theorem. Visibility is generally complex, and can be expressed as $\Gamma = V \exp(-j\phi)$, where V is the visibility amplitude and ϕ is the fringe phase. We ordinarily work with normalized visibility, i.e., $0 < V < 1$. With a two-element, single-beam (i.e., non-cophased) interferometer, the fringe phase is corrupted by the atmosphere and only the visibility amplitude is useful for imaging (typically, parametric imaging of compact sources; see, for example Boden *et al.* 1999; Mozurkewich *et al.* 1991). While phase and visibility are usually estimated via the same mechanism, the discussion here will be limited to estimation of the visibility amplitude.

This brief review will touch on visibility estimation via fringe scanning, the signal-to-noise ratio of the visibility estimator, estimator and atmospheric biases, and approaches to calibration.

7.2 Fringe Scanning and Matched Filtering

Visibility is just the contrast of the spatial fringe pattern. Most measurement schemes used with Michelson combiners use fringe scanning to convert the spatial fringe pattern to a

temporal one; demodulation of such a temporal signal presents a well-studied measurement problem. This problem occupies only a small niche in the larger field of phase-shifting interferometry for optical testing. The key aspects of the problem for stellar interferometry are accommodating the low intensity of the faint stellar source and the limitations of low-light-level detectors, so some of the more sophisticated phase-shifting algorithms are not readily applicable to our problem.

Fringe scanning to temporally encode the spatial fringe pattern can use step or continuous scanning. Generally, for fast scanning to follow atmospheric fringe motion, continuous scanning is used to avoid settling-time issues. Both sawtooth and triangular waveforms are used, depending on the problem (cf. Shao *et al.* 1988; Colavita *et al.* 1999). This is discussed further by in Section 8.4.4.

Visibility estimation can be analyzed from several perspectives; one is to just consider it a matched filter problem. The temporal fringe pattern for a normalized scan rate can be written as $I = N(1 + V \cos(t + \phi))$, where N is flux, V is visibility, and ϕ is fringe phase. This can also be written as the sum $N + X \cos(t) + Y \sin(t)$, where X and Y are the fringe quadratures. This signal is readily demodulated using the orthogonal basis functions $1, \cos(t), \sin(t)$; from estimates of $N, X,$ and Y we can compute the fringe phase and visibility. With integrating detectors, we must discretize the basis functions to limit the number of required reads (and attendant read noise), leading to, for example, four and eight-bin algorithms. For the common four-bin algorithm, we approximate sin and cos by quadrature squares waves; the basis functions remain orthogonal, but not optimal, and there is a 0.9 dB signal-to-noise penalty on bright stars. Figure 7.1 illustrates fringe estimation at PTI (Colavita *et al.*, 1999).

There is considerable literature on this subject; a number of references are given by Lawson at the end of Chapter 8.

7.3 Visibility Estimation and Signal-to-Noise Ratio

If the fringe phase is known, the fringe visibility can be estimated coherently using a coordinate rotation on the measured fringe quadratures, normalized by the flux. If the phase is unknown, we normally use an incoherent “energy” estimator. Starting with the latter, squared fringe visibility V^2 can be estimated using the four-bin algorithm as (see Colavita 1999)

$$V^2 = \frac{\pi^2}{2} \frac{\langle X^2 + Y^2 - \text{Bias} \rangle}{\langle N \rangle^2} \quad (7.1)$$

where the brackets refer to averaging over a number of samples, with the sample time chosen to freeze the atmospheric fringe motion. The standard deviation of the V^2 estimator, σ_{V^2} , can be calculated from the fourth-order statistics of Gaussian read noise and Poisson photon

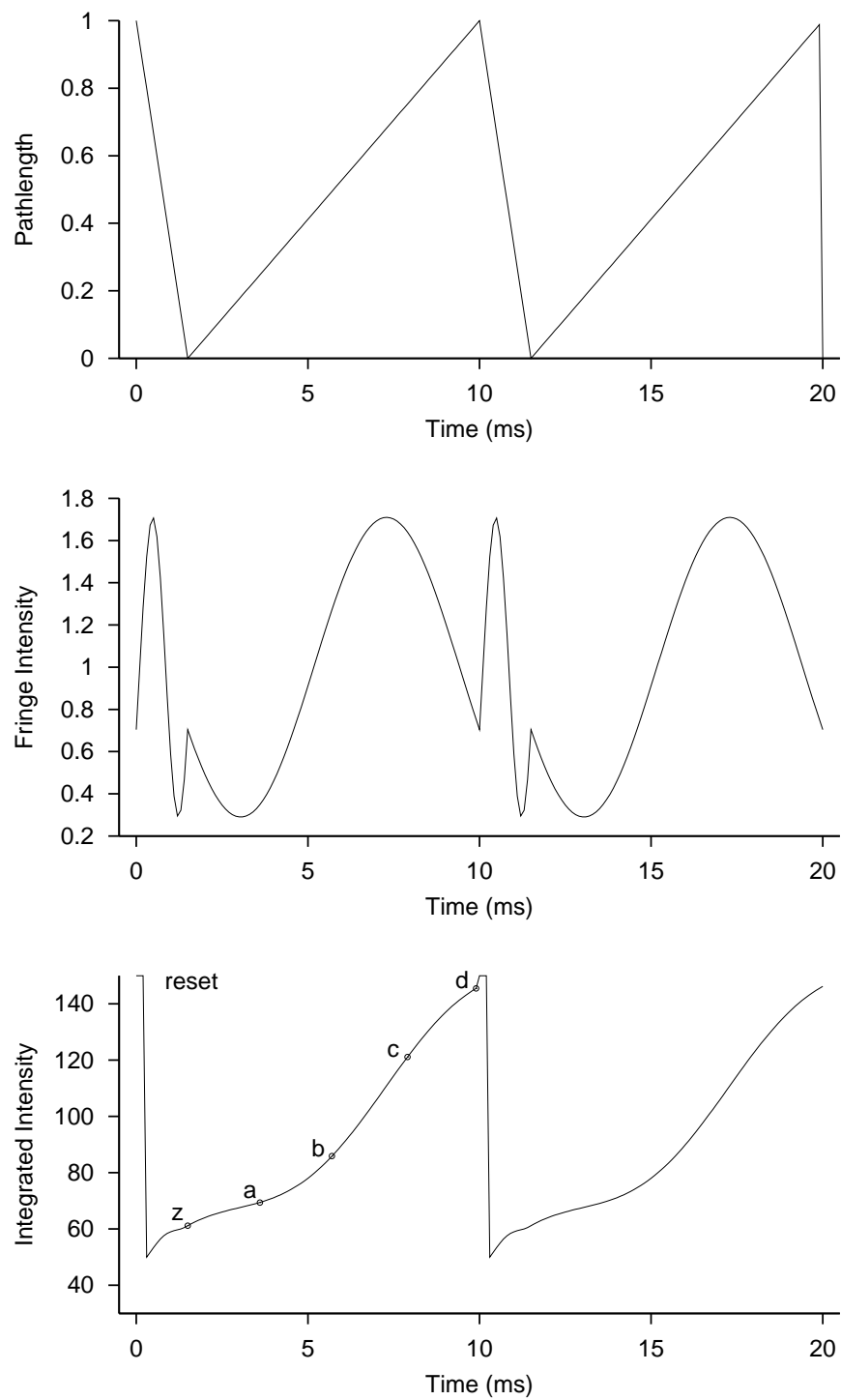


Figure 7.1: Fringe scanning with a sawtooth waveform at PTI.

noise processes. When photon-noise limited, the signal-to-noise ratio ($1/\sigma_{V^2}$) is

$$\frac{1}{\sigma_{V^2}} \propto \begin{cases} \sqrt{N}, & N \gg 1 \\ N, & N \ll 1 \end{cases}. \quad (7.2)$$

When read-noise limited (with read noise σ_{rn}), the signal-to-noise ratio is given by

$$\frac{1}{\sigma_{V^2}} \propto \left(\frac{N}{\sigma_{\text{rn}}} \right)^2, N \ll \sigma_{\text{rn}}^2. \quad (7.3)$$

Thus, as one becomes photon-noise starved or read-noise limited, the signal-to-noise ratio drops precipitously with decreasing light level as shown in Figure 7.2. The figure plots the signal-to-noise ratio for a single sample; the signal-to-noise ratio improves as the square root of the number of samples comprising the averages in Equation 7.1. However, especially when read noise is involved, there is a fairly steep wall, beyond which unreasonable numbers of samples are required to obtain a good final signal-to-noise ratio.

As mentioned above, if we know the fringe phase, we can use a coherent estimator. If we know the fringe phase in real-time, we can use phase referencing to increase the coherent integration time. If we know it a posteriori, we can use it to de-rotate and sum the fringe quadratures before computation of the visibility. Both approaches help move the detection problem away from the photon-starved or detector-noise-limited regimes.

Figure 7.3 illustrates the potential gain of coherently combining the fringe quadratures in groups of 10 samples before computing V^2 with Equation 7.1. Note that for high signal-to-noise ratios, coadding provides no benefit. More detail on this problem, and a number of references, are given by Colavita (1999).

7.4 Estimator Biases

For an accurate estimate of visibility, it is necessary to compensate for biases attributable to background, dark current, and detector imperfections. Also, as the V^2 estimator is an energy estimator, we must correct for biases attributable to squaring quantities which include noise. Bias-corrected visibility estimators are the first step in a data-calibration pipeline, which will also include periodic observation of calibrator objects.

The first set of V^2 biases are the offsets, or zero points, of the estimates of X , Y , and N ; these are typically calibrated through interspersed background measurements, i.e., measurement of the quantities when pointed at dark sky. While in principle X and Y should have no offsets, even in the presence of a finite background, in practice detector nonlinearities and reset tails introduce small offsets requiring calibration.

The second set of biases are the variances of the underlying Poisson photon-noise and Gaussian detector-noise processes which arise when squaring the fringe quadratures to compute the numerator of Equation 7.1. The photon noise bias takes the form $\langle X^2 + Y^2 \rangle =$

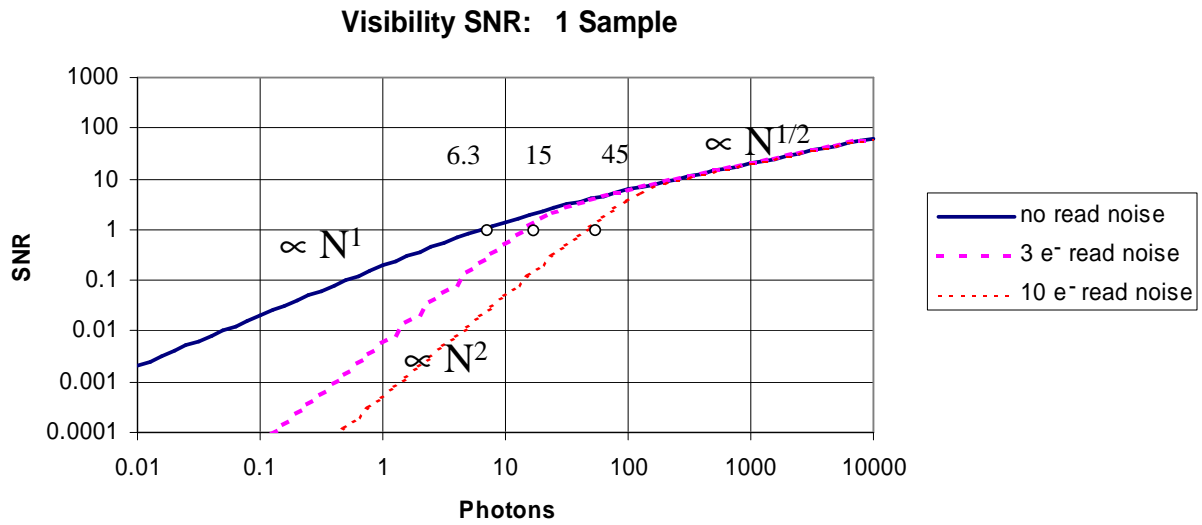


Figure 7.2: Signal-to-noise ratio of the V^2 estimator for 1 sample vs. photons per sample, for different amounts of read noise. 6.3, 15, and 45 electrons per sample are required to achieve an signal-to-noise ratio of 1 for the case of 0, 3, and 10 electrons read noise.

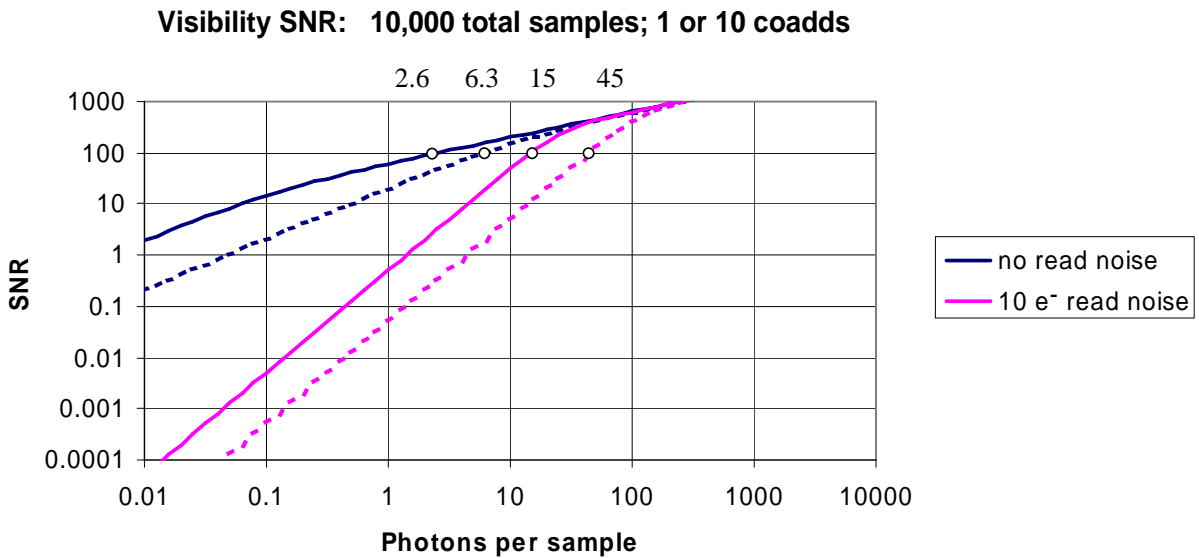


Figure 7.3: Signal-to-noise ratio of the V^2 estimator vs. photons per sample after averaging for 10,000 total samples, with and without coadding the phasors into groups of 10 samples before computing V^2 . With no read noise, a signal-to-noise ratio of 100 is achieved in 10,000 samples with 6.3 and 45 electrons per sample for the case of 0 and 10 electrons read noise, and with 2.6 and 15 electrons per sample when the phasors are coadded to groups of 10 before computing the visibility.

$k\langle N \rangle$, where k is the gain of the signal chain (counts/electron), with X , Y , and N in detector units. The read-noise bias takes the form $\langle X^2 + Y^2 \rangle = 4k^2\sigma_{\text{rn}}^2$, where the read noise variance is for a single double-correlated read (a four-bin algorithm has been assumed). These biases can be calibrated several ways: one approach is to determine the detector-noise term from $\langle X^2 + Y^2 \rangle$ as measured on dark sky, and the photon-noise term from the measured value of $\langle N \rangle$ and an estimate of k . The gain k can be readily determined from measurements of $\langle X^2 + Y^2 \rangle$ at two different light levels (see Colavita 1999).

It's important to note that, especially at low light levels, errors in measuring these variance terms can become the dominant error in estimating visibility, as the signal-to-noise ratio of these calibrations is the same as that of the measurements they are being used to calibrate. Thus observation planning must allocate sufficient integration time for the calibration measurements.

This topic is discussed in more detail in the context of PTI by Colavita (1999).

7.5 Atmospheric Biases

I can do no more than briefly touch on the effects of atmospheric biases; for more detail, see, for example Tango and Twiss (1980).

Atmospheric biases are challenging to calibrate to high precision as the atmospheric statistics are not stationary. The approach used by most groups is to minimize these biases through design or observing strategy; apply modest modeling, when appropriate, to compensate for first-order effects; and use rapid observations of calibrators to track the residual visibility variations.

7.5.1 Spatial Wavefront Errors

For slow guiding, the visibility reduction attributable to wavefront errors can be written

$$\langle V^2 \rangle = \exp[-2.06(d/r_0)^{5/3}], \quad (7.4)$$

where d is the subaperture diameter and r_0 is the atmospheric coherence diameter. This term can be reduced through fast guiding, or through the use of adaptive optics (AO). Except for a factor of 2 in the exponent, the Strehl of an AO system follows a similar expression, and the AO literature addresses this problem in detail (cf. Tyson 1997).

However, for interferometers, which usually process only a single spatial mode per aperture, the option exists to apply modal filters to correct the visibility reduction attributable to spatial wavefront errors. Single-mode optical fibers are often used for this purpose. They can be used either to filter the combined light from the two apertures, or to implement a fully fiber-optic beam combiner. As the fibers select only a single spatial mode, the visibility (attributable to wavefront errors only) is given by the scintillation formula $V^2 =$

$4I_1I_2/(I_1 + I_2)^2$, where I_1 and I_2 are the coupled intensities from each aperture into the fiber(s), which vary with fluctuations in the instantaneous wavefront distortion. For a post-combination fiber, one can show that only the average ratio of $\langle I_1 \rangle / \langle I_2 \rangle$ is needed to calibrate the residual V^2 reduction (Shaklan *et al.*, 1992). While it can be hard to get an accurate simultaneous measurement with this architecture, it is often adequate to use a nearby calibrator, assuming integration times long enough that only the systematic part of the ratio remains. Alternatively, this term can be calibrated through the use of a fully single-mode combiner, which simultaneously samples the coupled intensities from each aperture (Coudé du Foresto, 1994).

As an example, Figures 7.4 and 7.5 present data from PTI plotting V^2 vs. time for a number of sources during a night. Each point represents a 25-sec average. Of note is the difference in visibility between the broadband white-light channel, which is not spatially filtered, and the spectrometer channel (actually, a composite estimator of all of the spectrometer channels), which uses a post-combination single-mode spatial filter. On this night, use of the fiber doubles the measured V^2 .

7.5.2 Temporal Errors

For fringe tracking that is slow compared with the sample time (generally a good approximation), the visibility reduction attributable to fringe motion can be written

$$\langle V^2 \rangle = \exp[-(T/T_{0,2})^{5/3}], \quad (7.5)$$

where T is the coherent integration time and $T_{0,2}$ is the two-aperture variance-definition coherence time. While there are no modal filters applicable to temporal blurring, some compensation for this visibility reduction can be applied using contemporaneous measurements of the fringe phase motion. In particular, a visibility correction of the form $V^2 \rightarrow V^2 \exp(C_0 \sigma_{\Delta\phi}^2)$ can be applied, where $\sigma_{\Delta\phi}^2$ is the measured phase jitter during the observation interval, and C_0 is a scale factor which can be derived from an atmospheric model (see Colavita 1999).

7.5.3 Finite Coherence

The V^2 envelope with respect to delay x is just the magnitude squared of the Fourier transform of the system bandpass. For a rectangular bandpass,

$$V^2 \propto \text{sinc}^2\left(\frac{\pi x}{R\lambda}\right), \quad (7.6)$$

where λ is wavelength and R is the spectrometer resolution $R = \lambda/\Delta\lambda$. Thus for accurate visibility measurements, one must calibrate the shape of the envelope, or work in a narrow band. At PTI, we have found it convenient to combine the visibility estimates from several narrow-band spectrometer channels to synthesize a wide-band channel with a long effective coherence length.

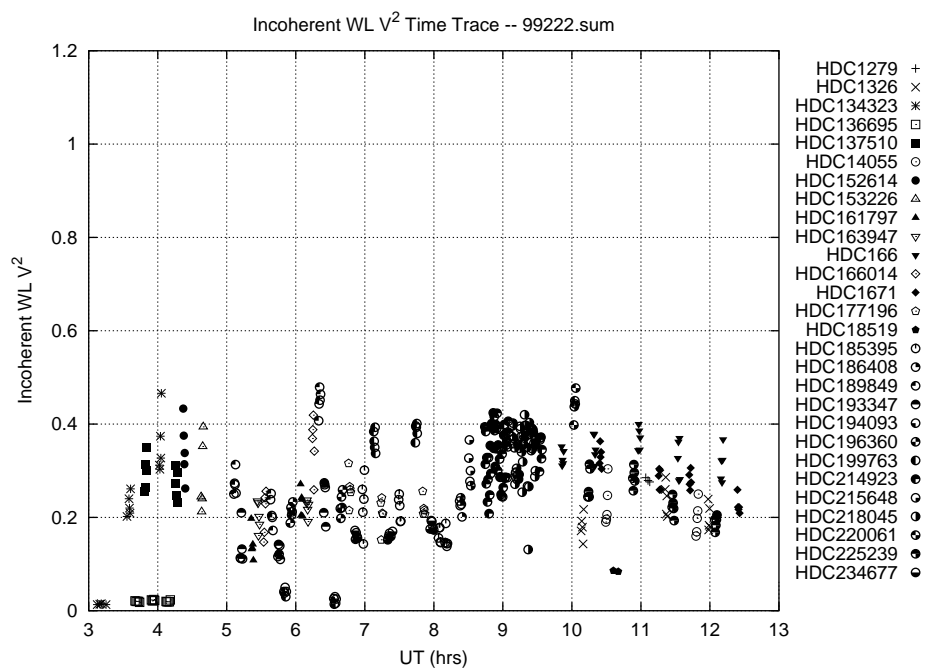


Figure 7.4: V^2 values from the white-light channel on PTI vs. time. Each point represents a 25-sec average.

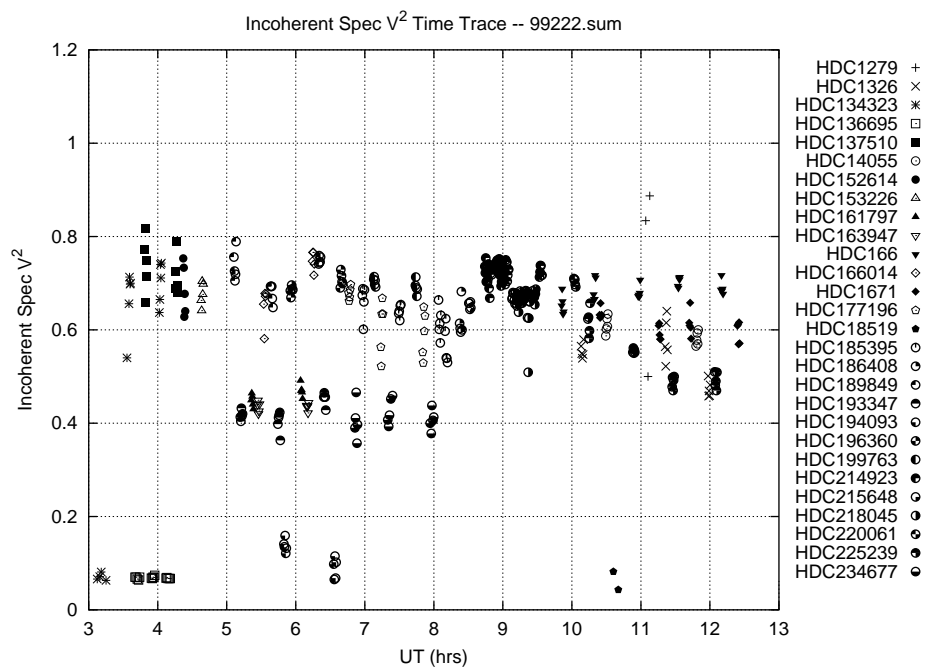


Figure 7.5: V^2 values from the spectrometer channel on PTI vs. time. Each point represents a 25-sec average of the composite spectral value.

7.5.4 Mismatched Stroke

Systematic errors accrue if the length of the pathlength-modulation stroke doesn't match the wavelength. This introduces errors in both the fringe phase and visibility estimates. However, it can be corrected through a transformation applied to the measured fringe quadratures (Colavita *et al.*, 1999).

7.6 Conclusion

With a two-element interferometer, the amplitude of the complex fringe visibility is the primary observable. By converting spatial fringe patterns to temporal ones, we reduce the measurement to a matched-filter problem that is readily solved. While we typically average a number of short exposures to provide a good visibility estimate, at low light levels the estimator statistics change from \sqrt{N} to N or N^2 , establishing an effective limiting magnitude. This magnitude can be increased through larger apertures with AO and longer coherent integration times with phase referencing. For the case of a fringe-tracking interferometer where the signal-to-noise limit is attributable to the use of narrow channels on the spectrometer side of the system, coherent visibility estimators can be used to improve the visibility estimates. No matter what type of estimator is used, accurate correction must be applied for biases in the estimator itself, as well as biases attributable to atmospheric and systematic errors.

Acknowledgments

This work was conducted at the Jet Propulsion Laboratory, California Institute of Technology, under contract with the National Aeronautics and Space Administration.

References

- A.F. Boden, C.D. Koresko, G.T. van Belle, M.M. Colavita, P.J. Dumont, J. Gubler, S.R. Kulkarni, B.F. Lane, D. Mobley, M. Shao, J.K. Wallace, and G.W. Henry, "The visual orbit of ι Pegasi," *Astrophys. J.* **515**, 356–364 (1999).
- M.M. Colavita, "Visibility estimators for the Palomar Testbed Interferometer," *Pub. Astron. Soc. Pac.* **111**, 111–117 (1999).
- M.M. Colavita, J.K. Wallace, B.E. Hines, Y. Gursel, F. Malbet, D.L. Palmer, X.P. Pan, M. Shao, J.W. Yu, A.F. Boden, P.J. Dumont, J. Gubler, C.D. Koresko, S.R. Kulkarni, B.F. Lane, D.W. Mobley, and G.T. van Belle, "The Palomar Testbed Interferometer," *Astrophys. J.* **510**, 505–521 (1999).
- V. Coudé du Foresto, "Integrated optics in astronomical interferometry," in *Very High Angular Resolution Imaging*, J.G. Robertson and W.J. Tango, eds., Proc. IAU Symp. 158, 261–271 (Dordrecht: Kluwer Academic, 1994).

- D. Mozurkewich, K.J. Johnston, R.S. Simon, P.F. Bowers, R. Gaume, D.J. Hutter, M.M. Colavita, M. Shao, and X.P. Pan, “Angular diameter measurements of stars,” *Astron. J.* **101**, 2207–2219 (1991).
- S.B. Shaklan, M.M. Colavita, and M. Shao, “Visibility calibration using single-mode fibers in a long-baseline interferometer,” in *High Resolution Imaging by Interferometry II*, J.M. Beckers and F. Merkle, eds., ESO Conf. and Workshop **39**, 1271–1283 (Garching, Germany: European Southern Observatory, 1992).
- M. Shao, M.M. Colavita, B.E. Hines, D.H. Staelin, D.J. Hutter, K.J. Johnston, D. Mozurkewich, R.S. Simon, J.L. Hershey, J.A. Hughes, and G.H. Kaplan, “The Mark III stellar interferometer,” *Astron. Astrophys* **193**, 357–371 (1988).
- W.J. Tango and R.Q. Twiss, “Michelson stellar interferometry,” *Prog. Opt.* **17**, 239–277 (1980).
- R.K. Tyson, *Principles of Adaptive Optics* (New York: Academic Press, 1997).